1 Drained and Undrained Triaxial Tests on Sand

The behavior of sands in triaxial state of stress is the focus of attention in this verification. Sands, while shearing in triaxial test, show a hardening behavior depending on the being loose, medium or dense show different in volumetric behavior. Loose sand undergoes compaction and medium dense and dense sand will show an initial compaction followed by dilation and increase in volume. In undrained triaxial test, due to the generation of excess pore water pressure, (very) loose sands will undergo static liquefaction. Dense sand on the other hand can endure high levels of shear stress due to the generation of negative excess pore water pressure. The Softenign/Hardening model in RS2 is adequate for simulating such behavior. Note that this model in its simplest form has one additional model parameter than that of the elasto-perfect-plastic Mohr Coulomb model.

Figures below show typical behavior of sands in drained and undrained triaxial tests. The graphs are obtained from RS2 simulations to demonstrate the range of behavior that could be simulated using the Softenign/Hardening model.

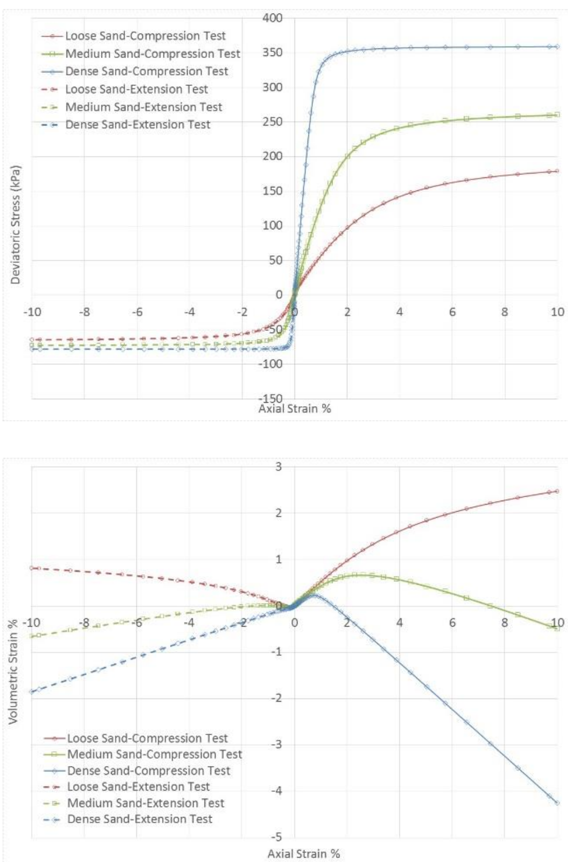

Drained triaxial compression and extension tests on loose, medium and dense sands; Variation of deviatoric stress and volumetric strain with axial strain.

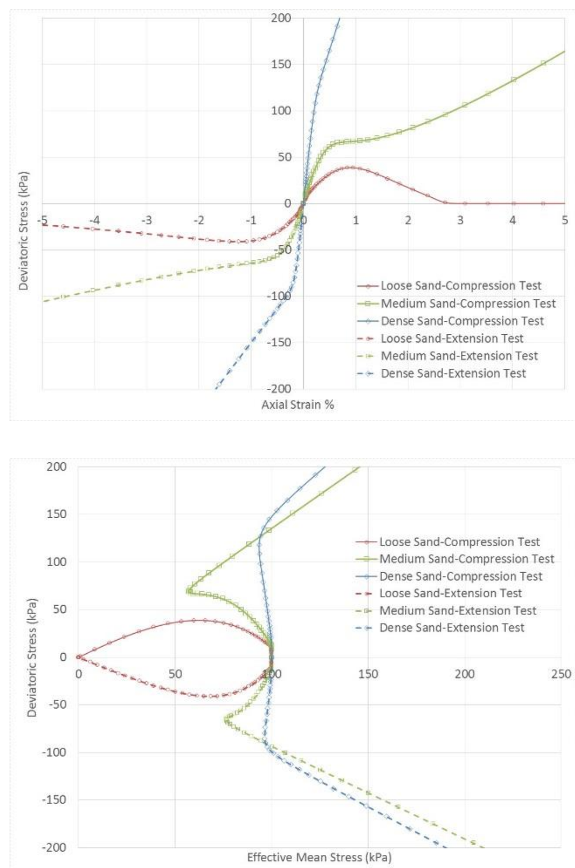

Undrained triaxial compression and extension tests on loose, medium and dense sands; Variation of deviatoric with axial strain, and the effective stress path.

1.1 Problem Description

Kolymbas and Wu [1] performed a series of triaxial tests on a variety of samples of granular materials; this included drained triaxial tests on loose and dense Karlsruhe sand. Similarly, Ashibli and Sture [2] completed triaxial tests on various samples of Ottawa sand under drained conditions. Schanz and Vermeer [3] also reported drained triaxial tests on Hostun sand in their work. In “Fundamentals of Plasticity in Geomechanics” [4], Pietruszczak presents the experimental results of undrained triaxial tests on Banding sand and on loose Reid Bedford sand.

In the following verification examples, the triaxial tests will be modeled using the Softening-Hardening model in RS2 and the results of these models will be compared with the experimental data. The material properties were not provided in the papers being examined, but it was possible to derive the values of the key parameters using the experimental results.

Figure 1 shows the loading for a triaxial test; a hydrostatic pressure is first applied and then an additional axial load is applied to the sample.

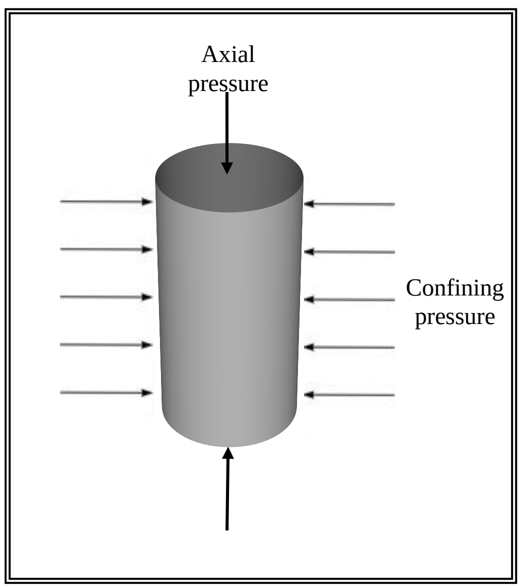

Figure 1: Loading conditions in a triaxial test

1.2 Experimental Data

As previously mentioned, the purpose of this verification is to compare the results of a RS2 model to experimental results for drained and undrained triaxial tests on sand. In the sources consulted, the results for the triaxial tests were provided in a number of different graphs.

In the first source consulted, Kolymbas and Wu [1], the authors performed drained triaxial tests on samples of loose and dense Karlsruhe sand. The results of the tests on the loose sand are presented below in a graph of stress ratio and volumetric strain versus axial strain.

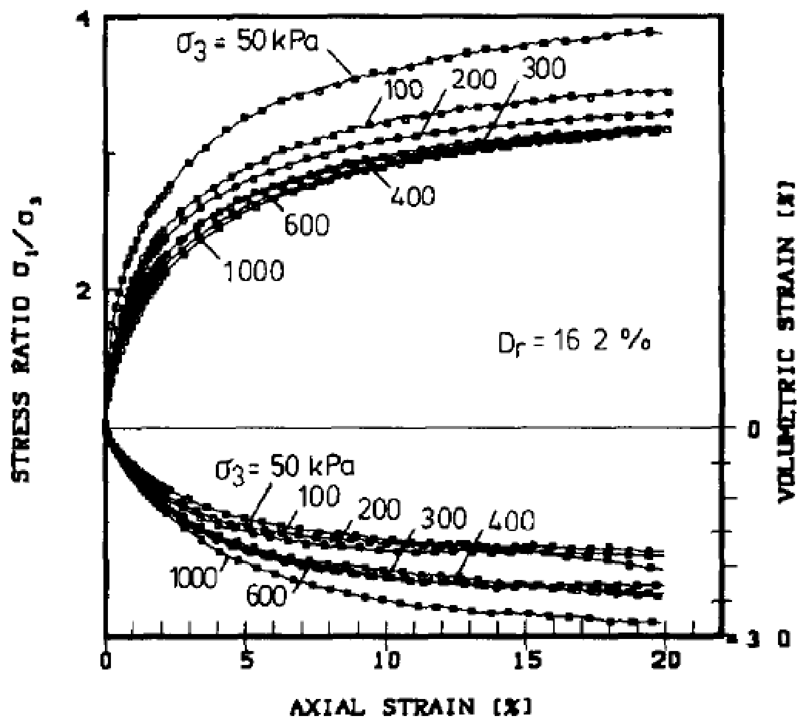

Figure 2: Experimental results of triaxial tests on loose Karlsruhe sand [1]

Alshibli and Sture [2] conducted drained triaxial tests on various Ottawa sands with different material properties; the three different types of sand were referred to as the F-sand, M-sand and C-sand. The following figure shows the graph of principal stress ratio versus axial strain for the four different samples of C-sand, which include loose (C1, C2) and dense (C3, C4) samples. These tests were conducted with confining stresses of 15 kPa (C1, C3) and 100 kPa (C2, C4).

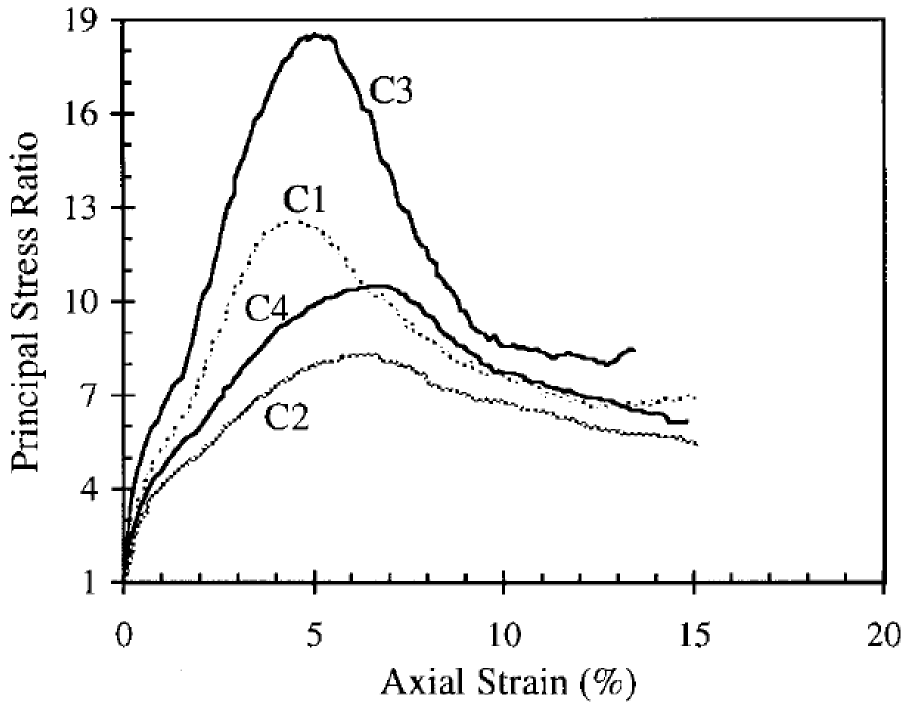

Figure 3: Graph of Principal Stress Ratio versus Axial Strain from the drained triaxial tests on various samples of C-Sand [2]

Schanz and Vermeer [3] reported drained triaxial tests on samples of both loose and dense Hostun sand, at a confining pressure of 300 kPa. For each test set-up, three tests were performed; the results indicate the variations between identical experimental tests. Figure 4 shows the results of the triaxial test on the dense Hostun sand.

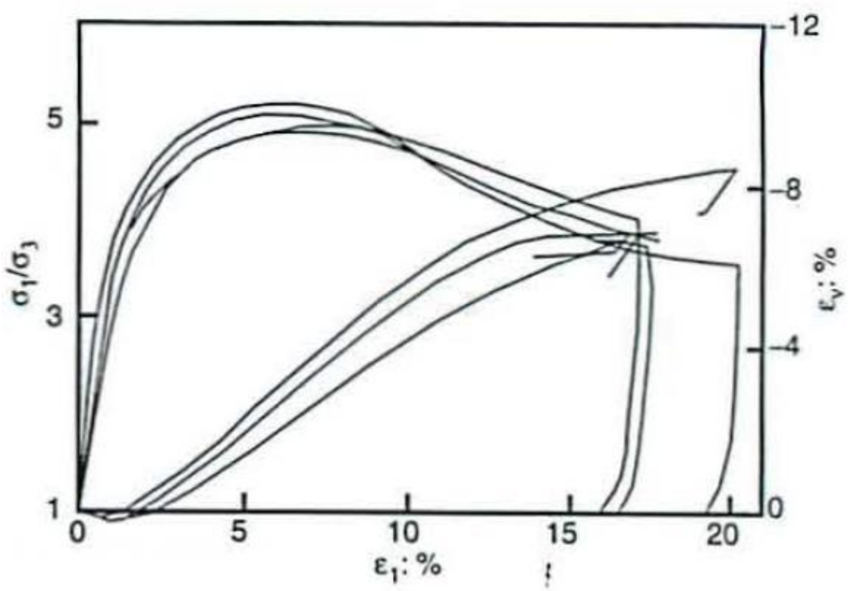

Figure 4: Graph of Principal Stress ratio and Volumetric Strain versus Axial Strain for the dense Hostun sand [3]

In “Fundamentals of Plasticity in Geomechanics” [4], Pietruszczak presents experimental results from triaxial tests on a large variety of different samples of sand. Figure 5 shows the results of triaxial tests on very loose Banding sand in the form of a p-q graph. This test was performed at a confining pressure of 400 kPa.

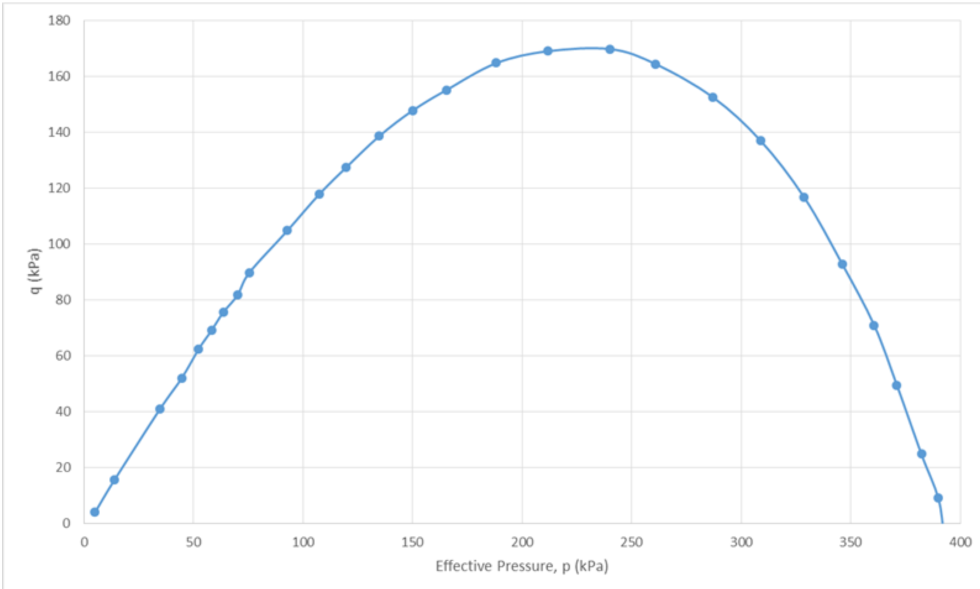

Figure 5: Graph of Deviatoric Stress versus Effective Pressure using the experimental data from the triaxial test on the Banding sand [4]

In [4], Pietruszczak also presents experimental results from triaxial tests on loose Reid Bedford sand. Figure 6 shows a graph of Deviatoric Stress versus Deviatoric Strain for this triaxial test. This test was performed at confining pressures of 275 kPa and 550 kPa.

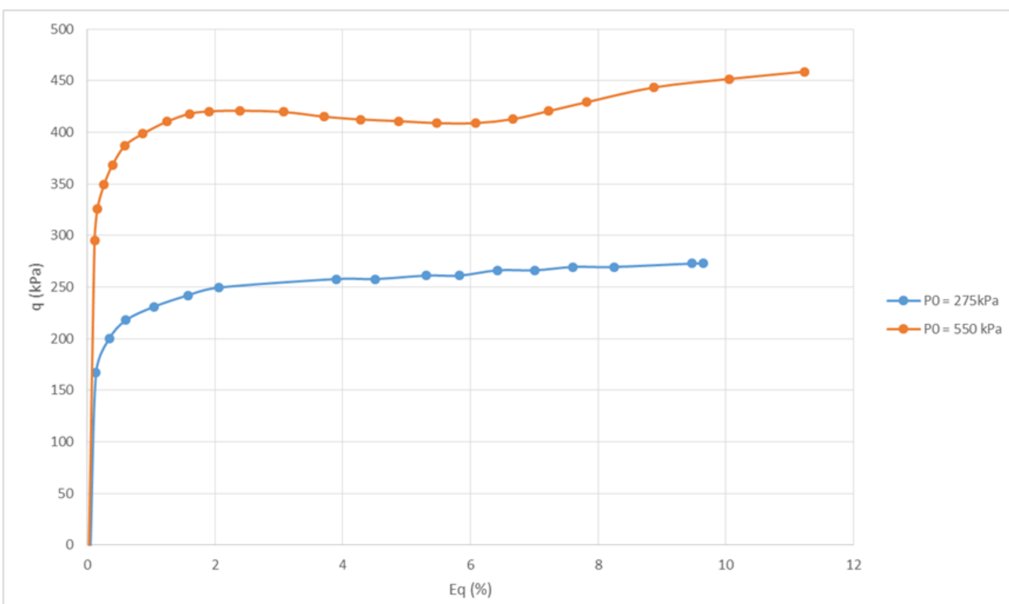

Figure 6: Graph of Deviatoric Stress versus Deviatoric Strain from the experimental results of the triaxial tests on loose Reid Bedford sand at confining pressures of 275 kPa and 550 kPa [4]

1.3 RS2 Model

In all of the references used, the material properties for the sands used in the triaxial tests were not provided. However, it was possible to derive the key properties from the experimental data. The following tables show the key material properties for the Karlsruhe sand, Ottawa Sand, Hostun sand, Banding sand and Reid Bedford sand.

Sand	Failure Friction Angle	Zero Dilation or Dilation Angle	Cohesion (kPa)	Hardening Parameter
Loose Karlsruhe	30.9°	30°	9.3	0.0075
Dense Karlsruhe	38.5°	26°	31.2	0.003
Ottawa C1	58.4°	18°	0	*
Dense Hostun	30°	30°	0	*
Loose Hostun	35°	33.5°	0	0.0038
Banding	31.5°	31.5°	0	0.0075
Loose Reid-Bedford	28.0°	27.5°	10.2	0.0015

Table 1: Summary of Material Properties for the different types of sand.

Note: For the Ottawa C-Sand a tabular hardening function was defined, rather than assigning a single value for the hardening parameter. This is due to the fact that the C-Sand exhibits some softening behavior. The following figure shows the friction angle versus deviatoric plastic strain function used to define the hardening behavior.

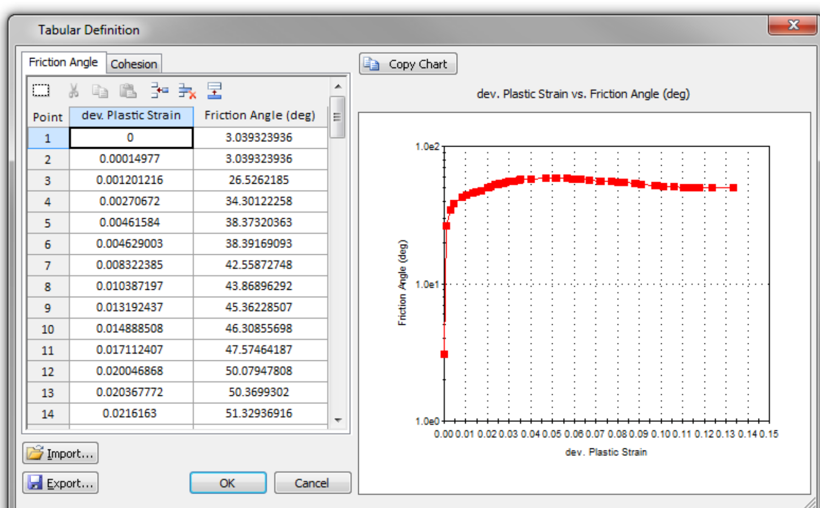

Figure 7: Tabular hardening function used for the loose Ottawa C-Sand (C1)

Similar to the Ottawa sand, a tabular hardening function was defined for the dense Hostun sand, rather than using the hardening parameter. The following figure shows the friction angle versus deviatoric plastic strain tabular hardening function for the Hostun sand.

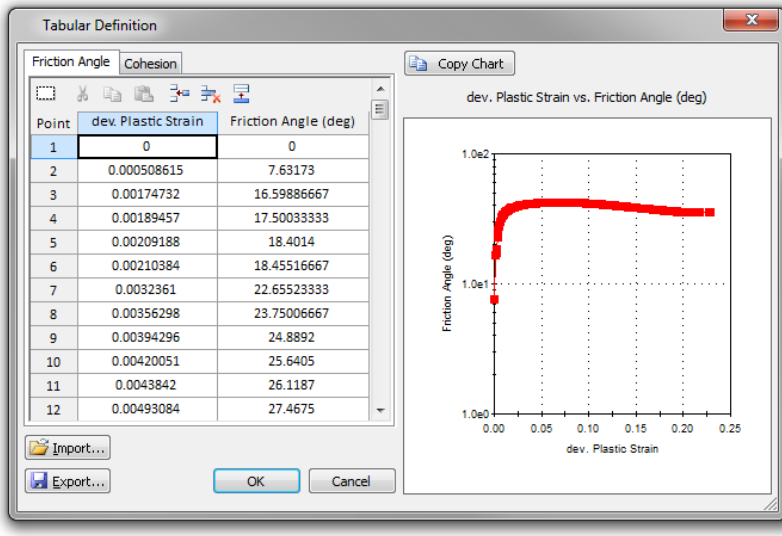

Figure 8: Tabular hardening function used for the dense Hostun sand.

The triaxial test setup was modelled in RS2 using an axisymmetric cylinder with unit height. In order to model the confining stress applied in the triaxial test, a constant field stress was used with the horizontal and vertical stresses set equal to the confining stress, and distributed loads equal to the confining stress were applied on the boundaries of the axisymmetric model. Figure 9 shows the field stress properties assigned for the Banding sand triaxial test, for which a 400 kPa confining stress was used.

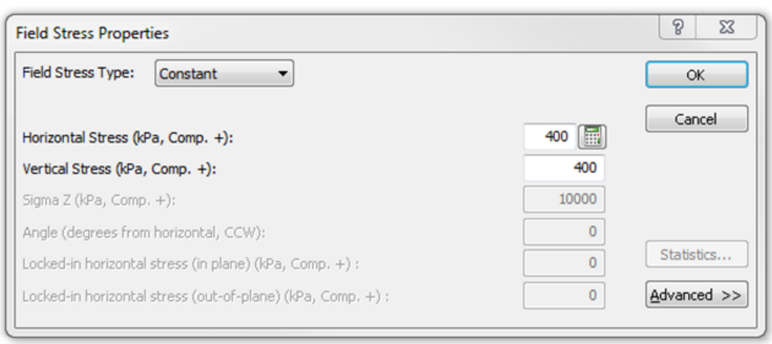

Figure 9: Field stress properties used in the RS2 model for the Banding sand triaxial test

The application of the axial load in triaxial testing was modeled by applying incremental displacements over 50 stages until the maximum axial strain from the experimental data was reached. Figure 10 shows the model geometry and incremental displacement applied in the drained triaxial test on the Karlsruhe sand. In the undrained tests it is assumed that no pore water is able to escape and thus no volume change can occur since water is incompressible. Therefore, in addition to the vertical displacement increment, a horizontal displacement increment was applied to maintain constant volume. Figure 11 shows the model geometry and displacement increments for the undrained test on the Banding sand.

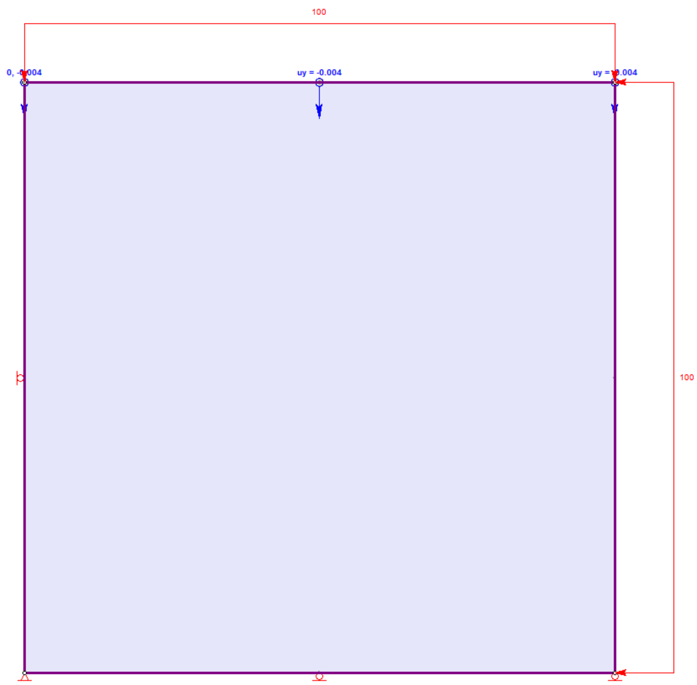

Figure 10: Typical RS2 model geometry and incremental displacement applied for drained triaxial tests

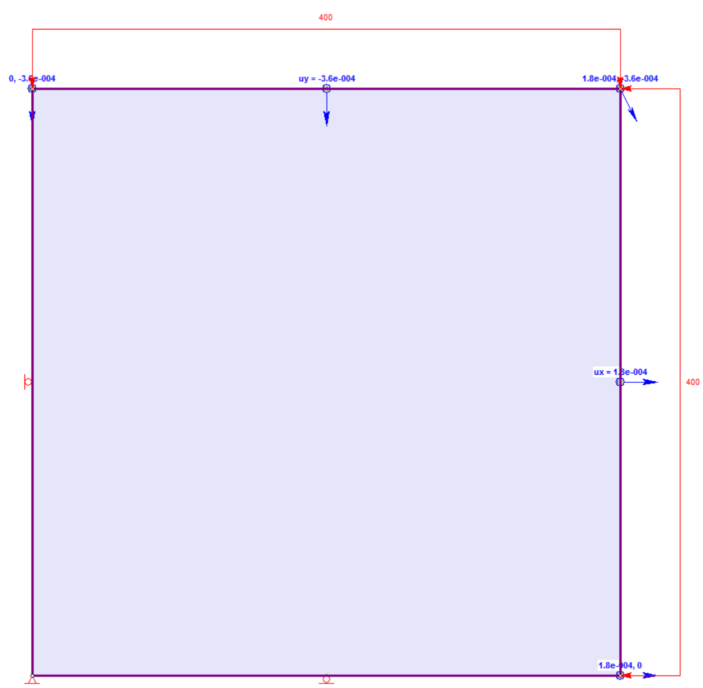

Figure 11: Typical RS2 model geometry and incremental displacement applied for undrained triaxial tests.

1.4 Results

1.4.1 Drained Triaxial Tests

1.4.1.1 Loose Karlsruhe Sand

The following figure compares the graphs of Stress Ratio versus Axial Strain between the experimental data and the results from the RS2 model. As seen in this figure, the results are in close agreement.

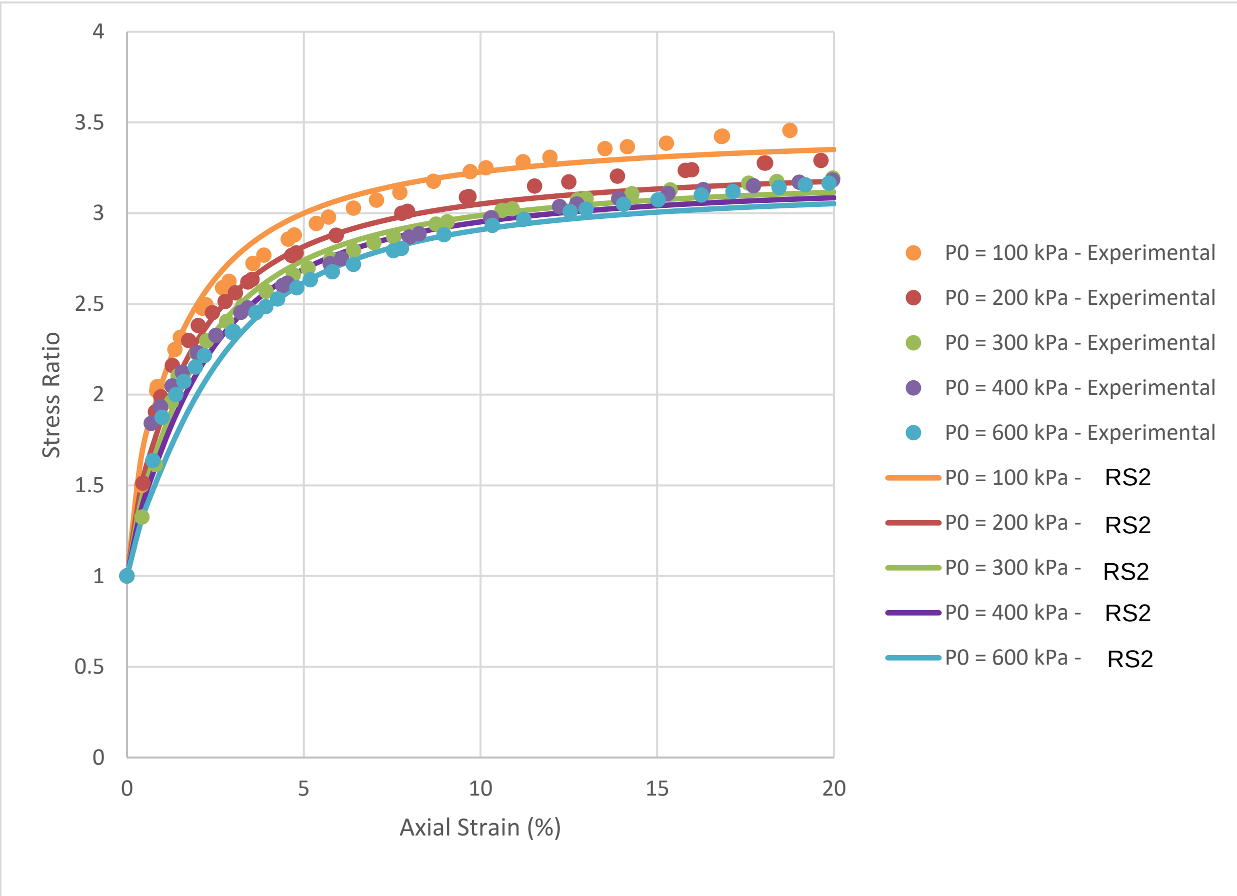

Figure 12: Stress Ratio versus Axial Strain for the experimental data and the RS2 model results for the loose Karlsruhe sand.

Figure 13 shows the graphs of volumetric strain versus axial strain for both sets of results. As can be seen in this figure, there are some discrepancies between the experimental data and the RS2 model results. This may be due to the fact that the elastic modulus is dependent on stress, but in this analysis a constant value of the Young's modulus was used. In addition, since experimental data is being used there will inevitably be some discrepancies.

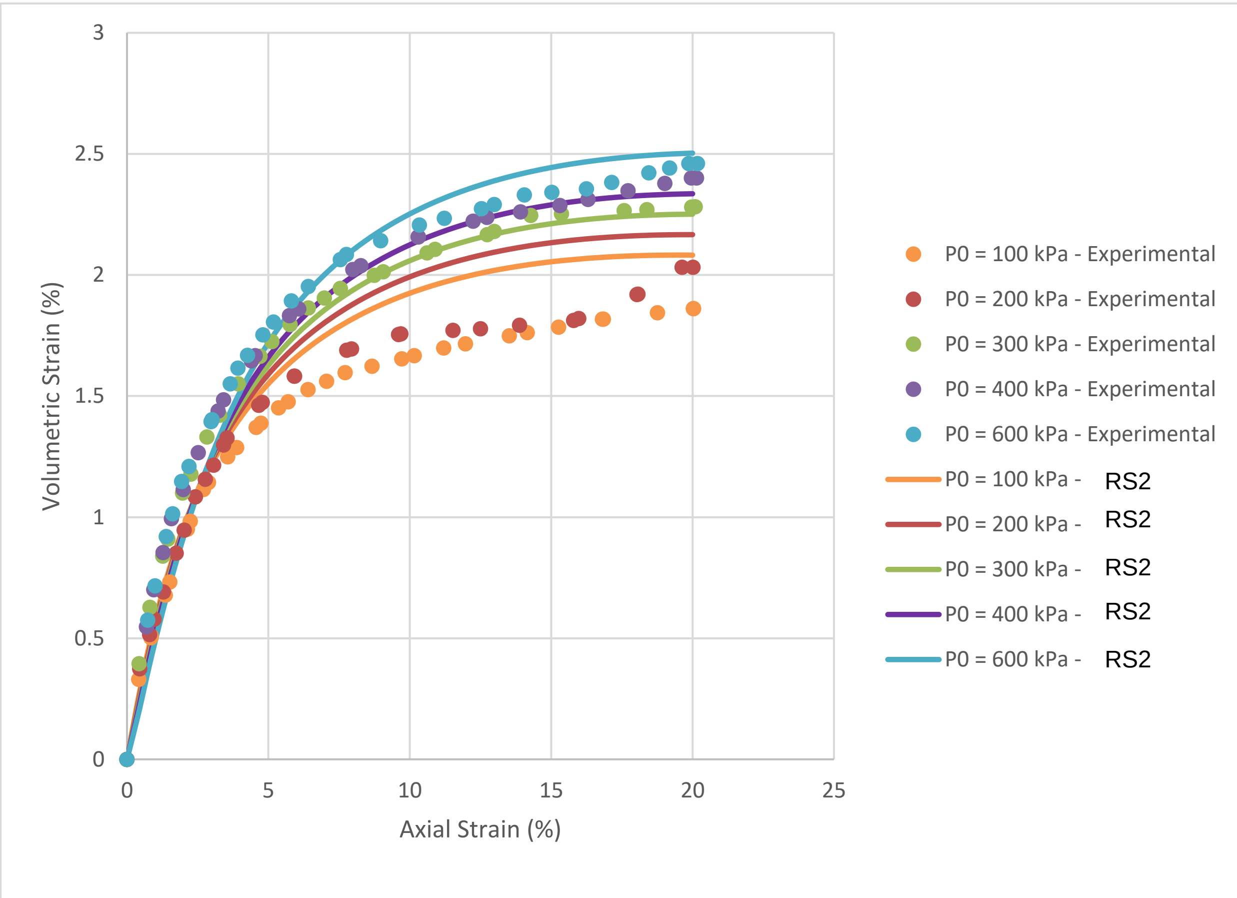

Figure 13: Volumetric Strain versus Axial Strain for the experimental data and the RS2 model results for the loose Karlsruhe Sand.

The next figure compares the deviatoric stress versus axial strain graphs between the experimental data and the RS2 model results. Similar to Figure 12, the results are in close agreement between RS2 and the experimental data.

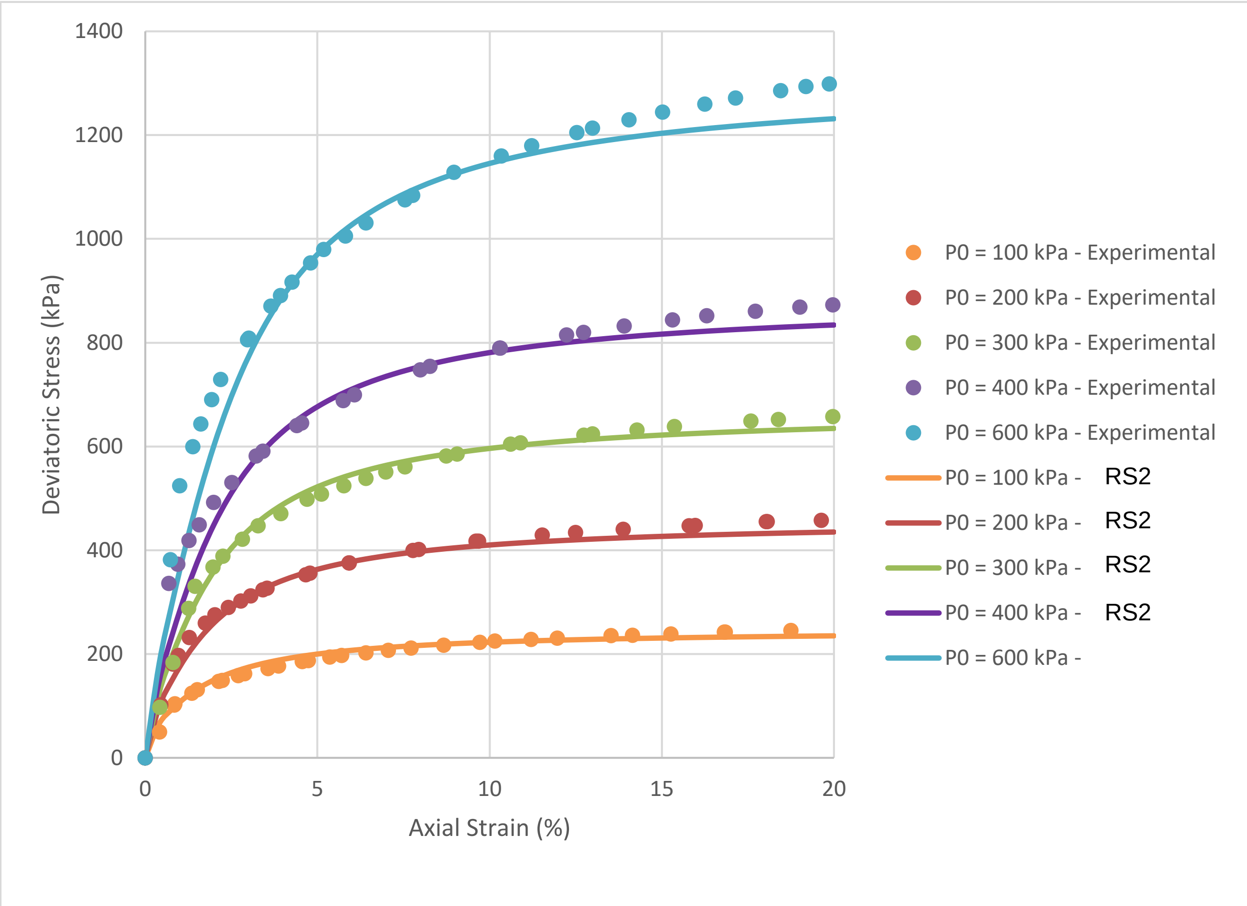

Figure 14: Deviatoric Stress versus Axial Strain for the experimental data and the RS2 model results for the loose Karlsruhe sand.

1.4.1.2 Dense Karlsruhe Sand

Figure 11 shows the graphs of deviatoric stress versus axial strain for the different confining pressures, comparing the results from the RS2 model with the experimental data. The results from the RS2 model are in close agreement with the experimental results.

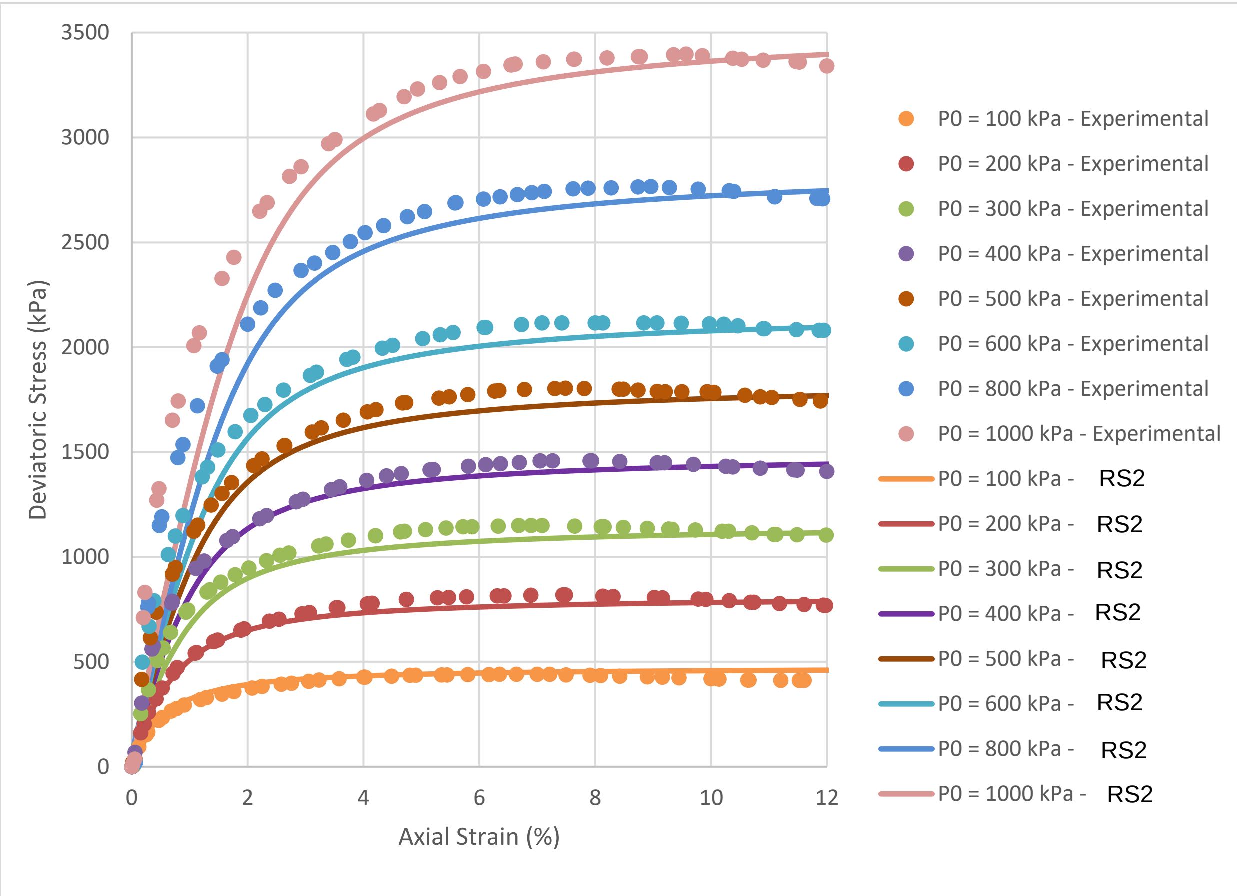

Figure 15: Graph of Deviatoric Stress versus Axial Strain for the dense Karlsruhe sand, comparing the results of the RS2 model with the experimental data

The following figure compares the graphs of volumetric strain versus axial strain for the RS2 model results and the experimental data. Similar to the graph of volumetric strain versus axial strain for the loose Karlsruhe sand, there are differences between the RS2 results and the experimental data. This is likely a result of the fact that a constant value of Young's modulus was used in the model, while it is actually dependent on stress.

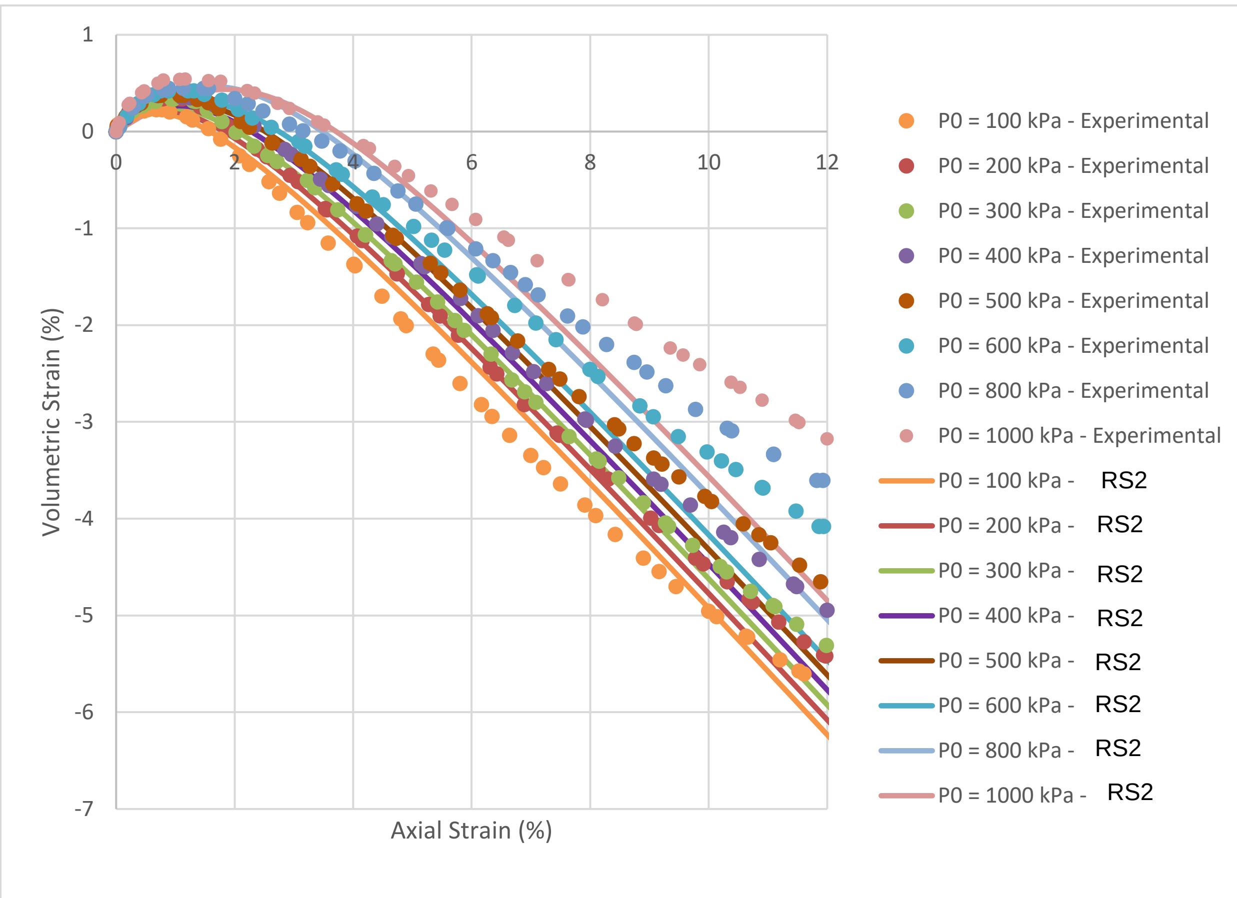

Figure 16: Graph of volumetric strain versus axial strain for the dense Karlsruhe sand, comparing the results of the RS2 model with the experimental data.

Widulinski et al. simulated the experimental triaxial tests on dense Karlsruhe sand from [1] using the discrete element method; they used a 3D discrete element model called YADE [5]. Figure 17 compares the graphs of the major principal stress (σ_1) versus axial strain for the 200 kPa confining stress test on the dense Karlsruhe sand for the RS2 model, the DEM model, and the experimental results. As shown by the graph, both the RS2 model and the DEM model results are in close agreement with the experimental data.

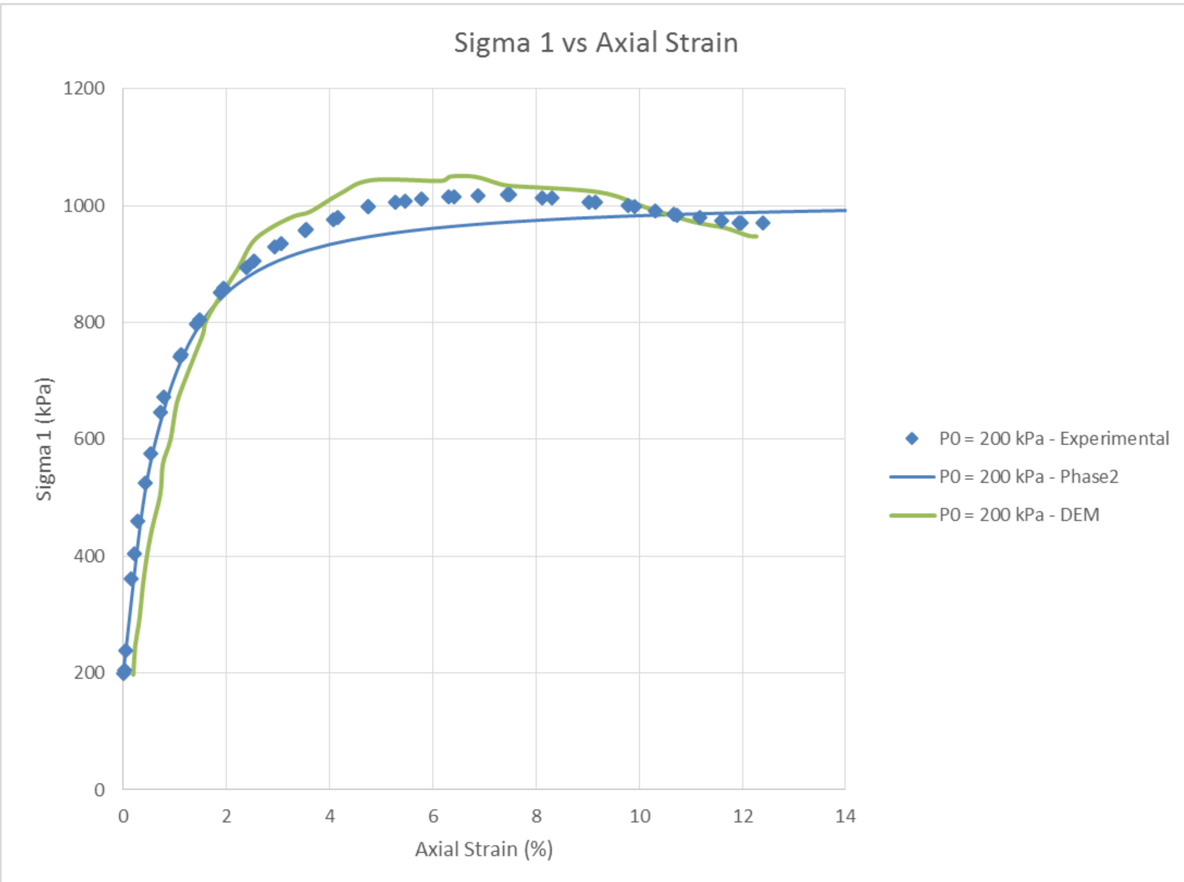

Figure 17: Graph of Major Principal Stress versus Axial Strain for the dense Karlsruhe sand, comparing the results of the RS2 model, the DEM model, and the experimental data.

The next figure shows the graphs of Volumetric Strain versus Axial Strain for the experimental data, as well as the RS2 model and DEM model results. The DEM model results are in closer agreement with the experimental data, but the RS2 model results are in good agreement with the data as well.

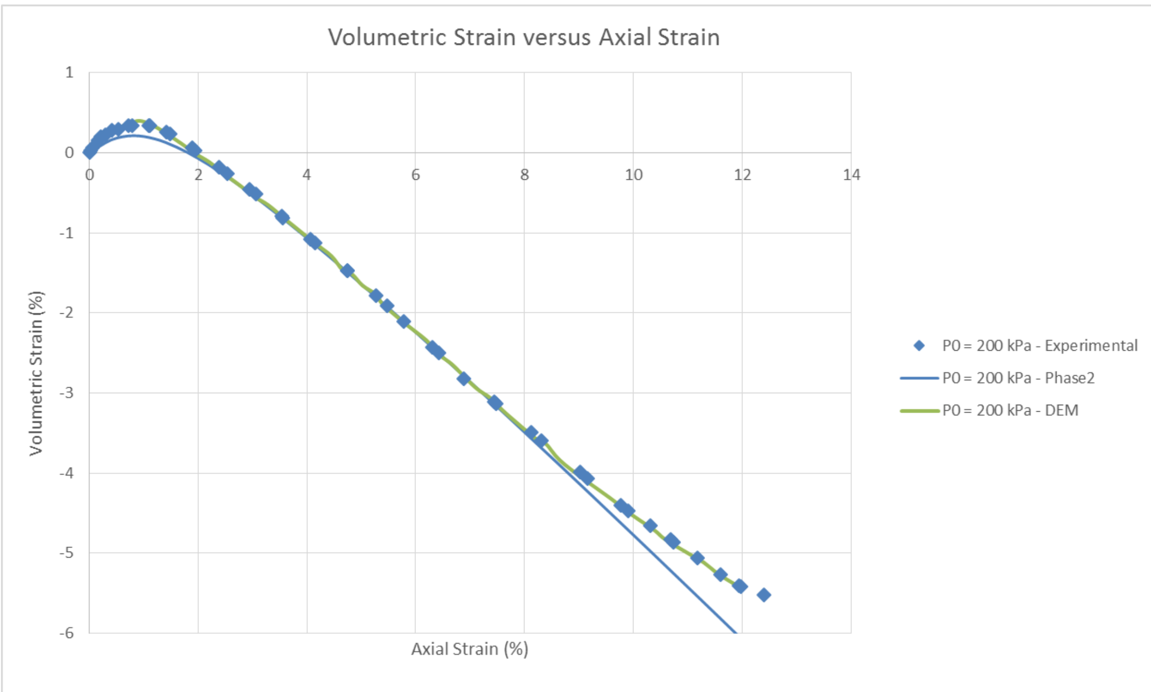

Figure 18: Graph of Volumetric Strain versus Axial Strain for the dense Karlsruhe sand, comparing the results of the RS2 model, DEM model and the experimental data.

1.4.1.3 Loose Ottawa C-Sand

Figure 19 shows the graph of Principal Stress Ratio versus Axial Strain for the C1 sample of Ottawa C-Sand, which as previously mentioned is a loose sand used in a triaxial test at a confining stress of 15 kPa. As shown in the figure below, the results of the RS2 model are in close agreement with the experimental data.

When considering the trends in Fig. 19, it should be noted that it has not been definitively determined whether or not the trends in post-yield behavior observed in laboratory testing should be used in the development of constitutive models. Beyond the yield point, the behavior observed in laboratory testing, which commonly called softening behavior, becomes increasingly dependent on the characteristics of the loading system and the development of localized fracture and shear zones. As such, flow rules developed based on laboratory testing data should be used with caution. Regardless, this verification is to demonstrate the flexibility of the Softening/Hardening model in simulating the observed behavior very closely.

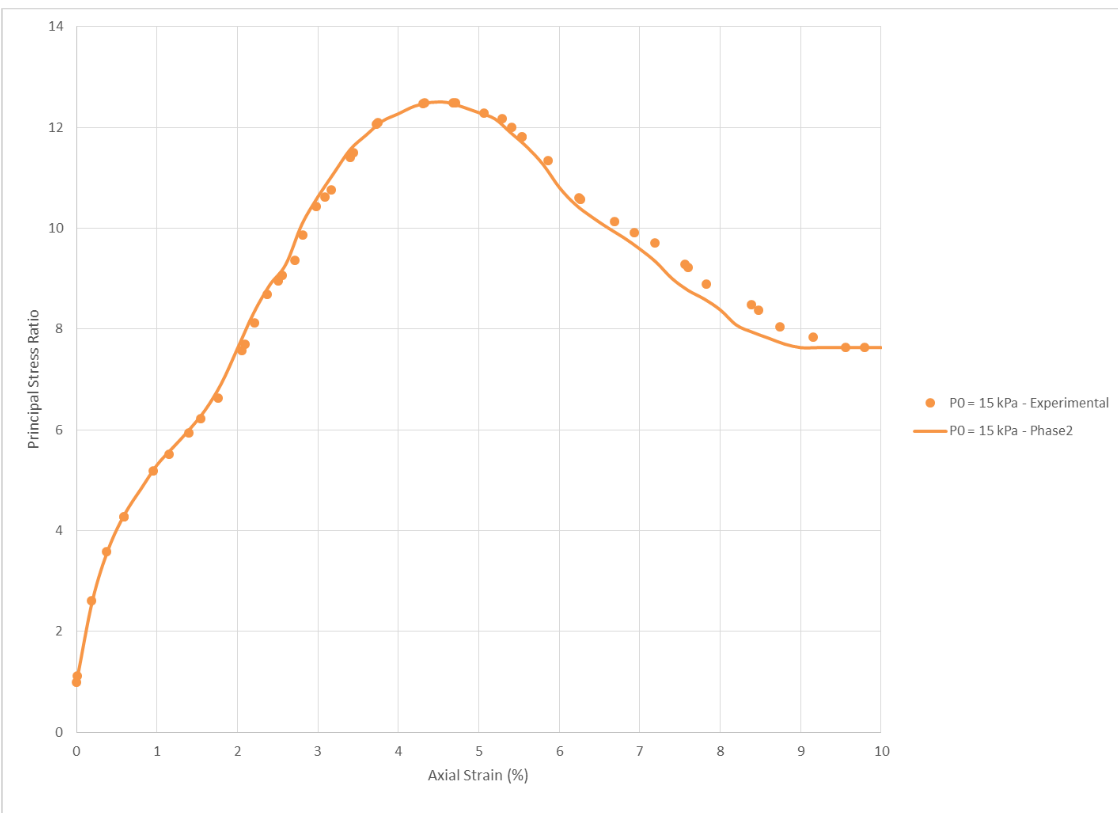

Figure 19: Graph of Principal Stress Ratio versus Axial Strain for the loose Ottawa C-Sand, comparing the results of the RS2 model with the experimental data.

The next figure shows the graph of Volumetric Strain versus Axial Strain for the Ottawa C-Sand, comparing the RS2 model results with the experimental data. As was the case with the Karlsruhe sand tests, there are some differences between the RS2 results and the experimental data for this graph. This is likely due to the reasons mentioned above.

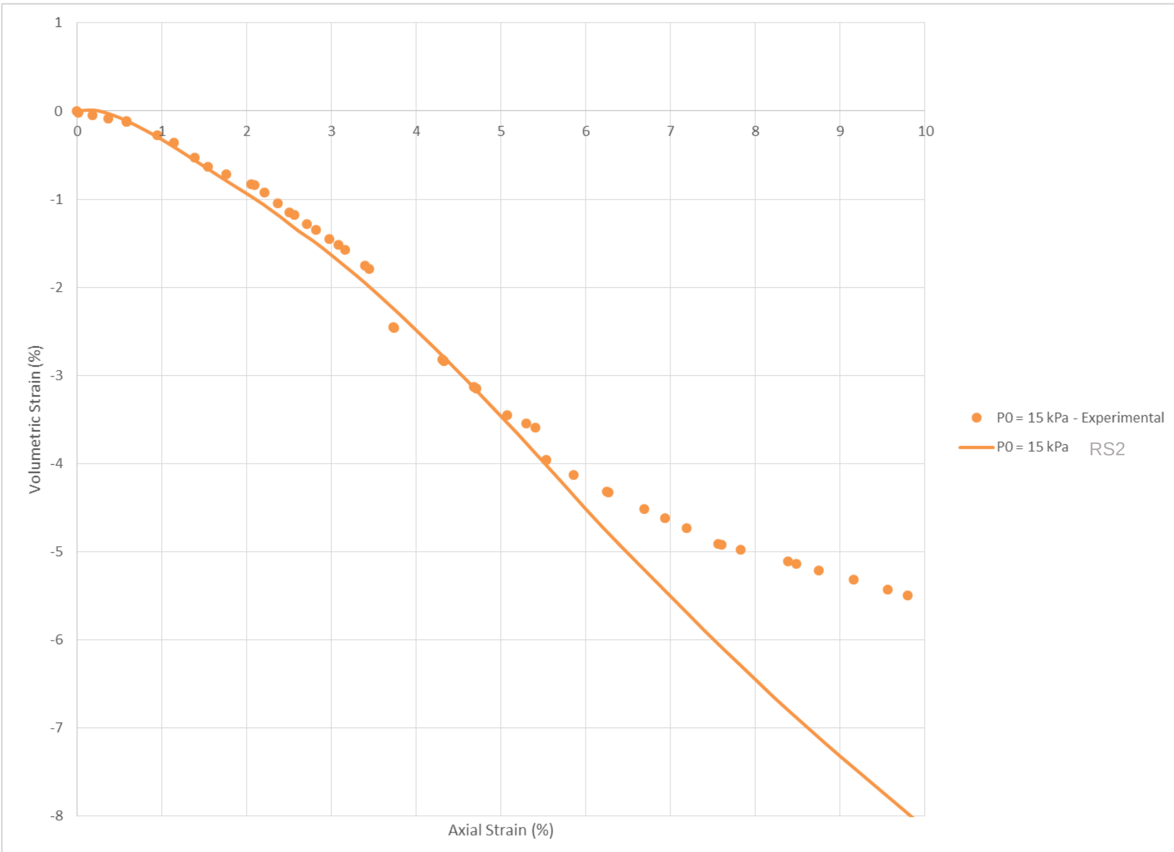

Figure 20: Graph of Volumetric Strain versus Axial Strain, comparing the RS2 model results with the experimental data for the C1 sample of Ottawa C-Sand.

Figure 21 compares the graphs of Deviatoric Stress versus Axial Strain for the two sets of results. Similar to Figure 19, the results are in close agreement.

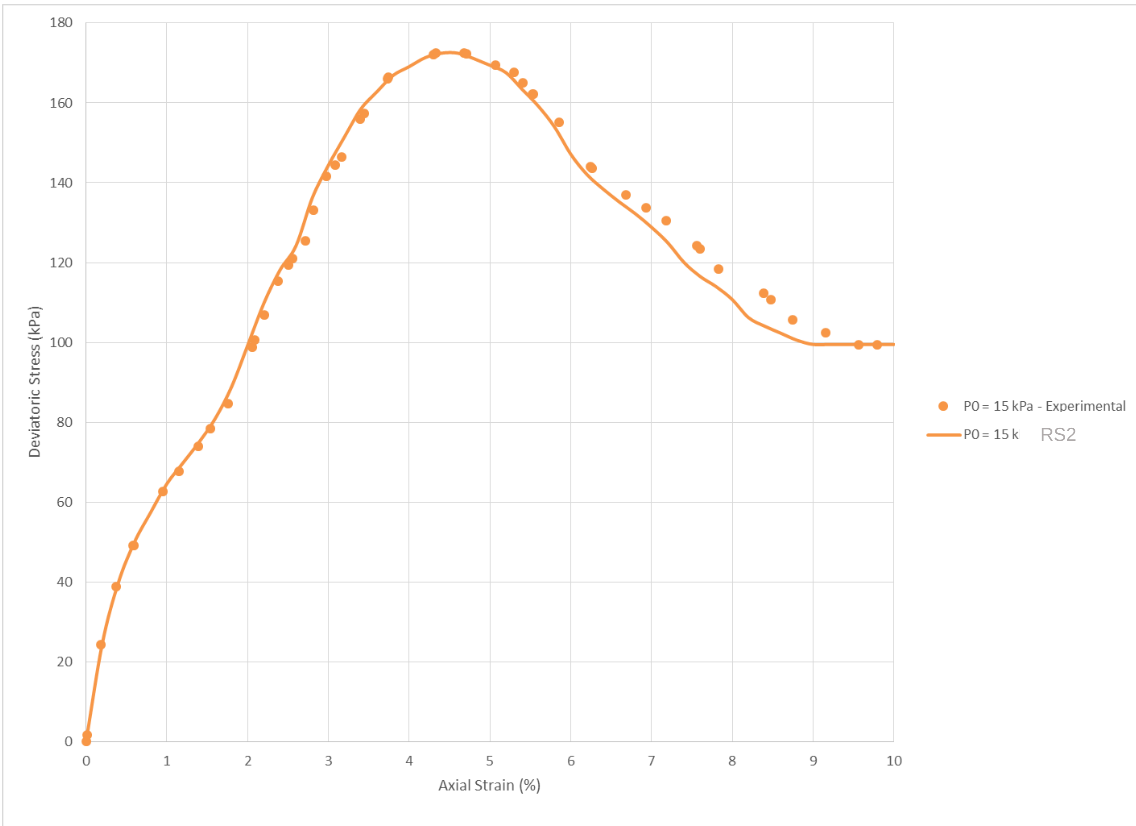

Figure 21: Graph of Deviatoric Stress versus Axial Strain for the C1 Ottawa C-Sand, comparing the results of the RS2 model with the experimental data.

1.4.1.4 Dense Hostun Sand

The first figure compares the graphs of Deviatoric Stress versus Axial strain for RS2 results and the experimental data for the dense Hostun sand. There are three sets of experimental data; these correspond to three different tests conducted on samples with the same properties at the same confining stress. There are two sets of RS2 results; one in which a tabular hardening function was defined, and one in which the hardening parameter *A* was used. As seen in Figure 22, the RS2 model results using the tabular function appear to agree with the average of these tests, since the curve falls approximately in the middle of the three sets of experimental data.

These results are also compared with the results of a PLAXIS model, taken from the PLAXIS material models manual [6]. The PLAXIS results were obtained using the hardening soil model. The RS2 results using the tabular hardening function agree with the experimental data better than the PLAXIS results, as the PLAXIS results do not capture the softening behavior. The RS2 results that do not use the tabular function are similar to the PLAXIS results.

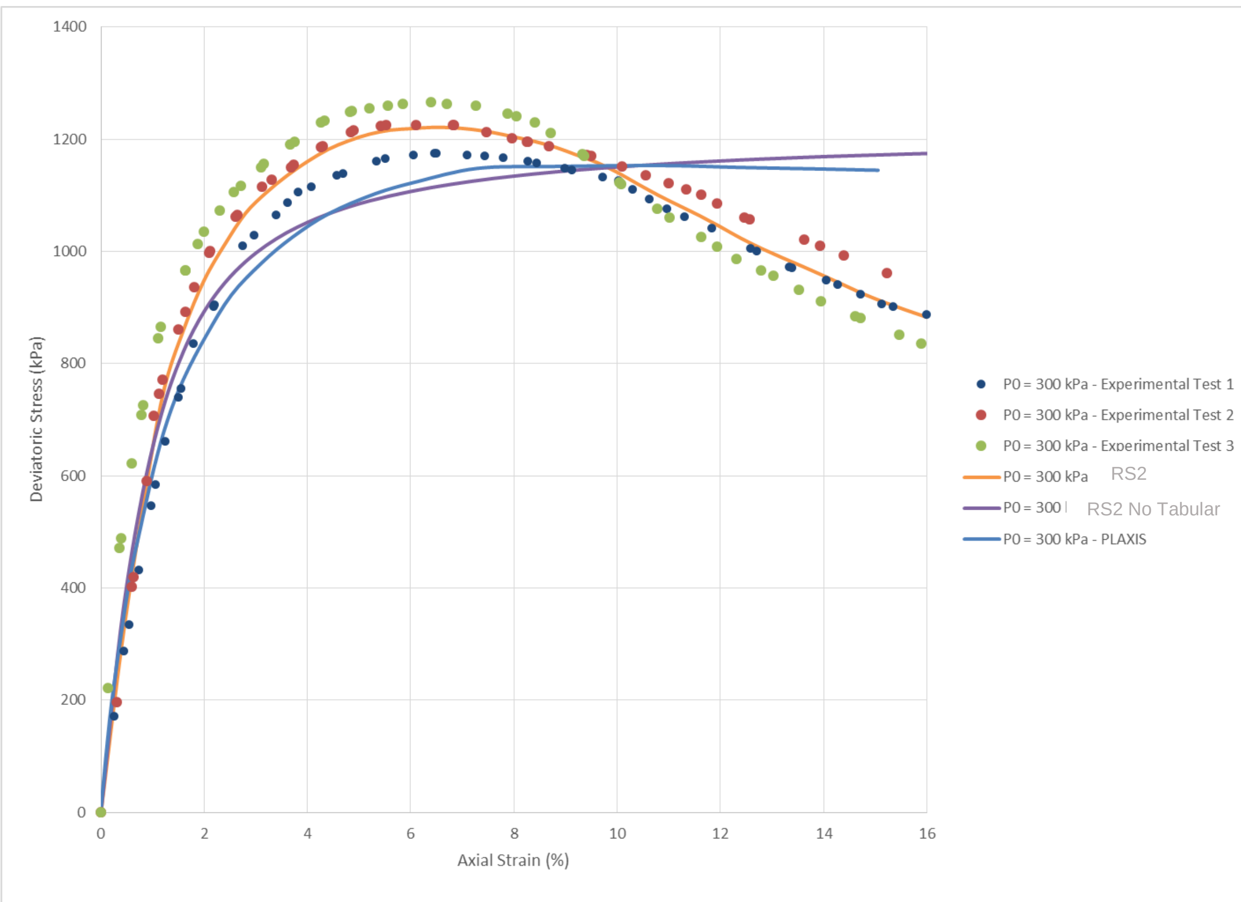

Figure 22: Graph of Deviatoric Stress versus Axial Strain, comparing the results of the RS2 model, PLAXIS model and the experimental data for the dense Hostun sand.

The next figure shows the graph of Volumetric Strain versus Axial Strain for the dense Hostun sand. Unlike the previous drained triaxial tests, the graph of Volumetric Strain for the RS2 model results is in close agreement with the experimental data. Once again, the RS2 results using the tabular hardening function agree with the experimental data better than the PLAXIS results, while the RS2 results that do not use the tabular function are similar to the PLAXIS results.

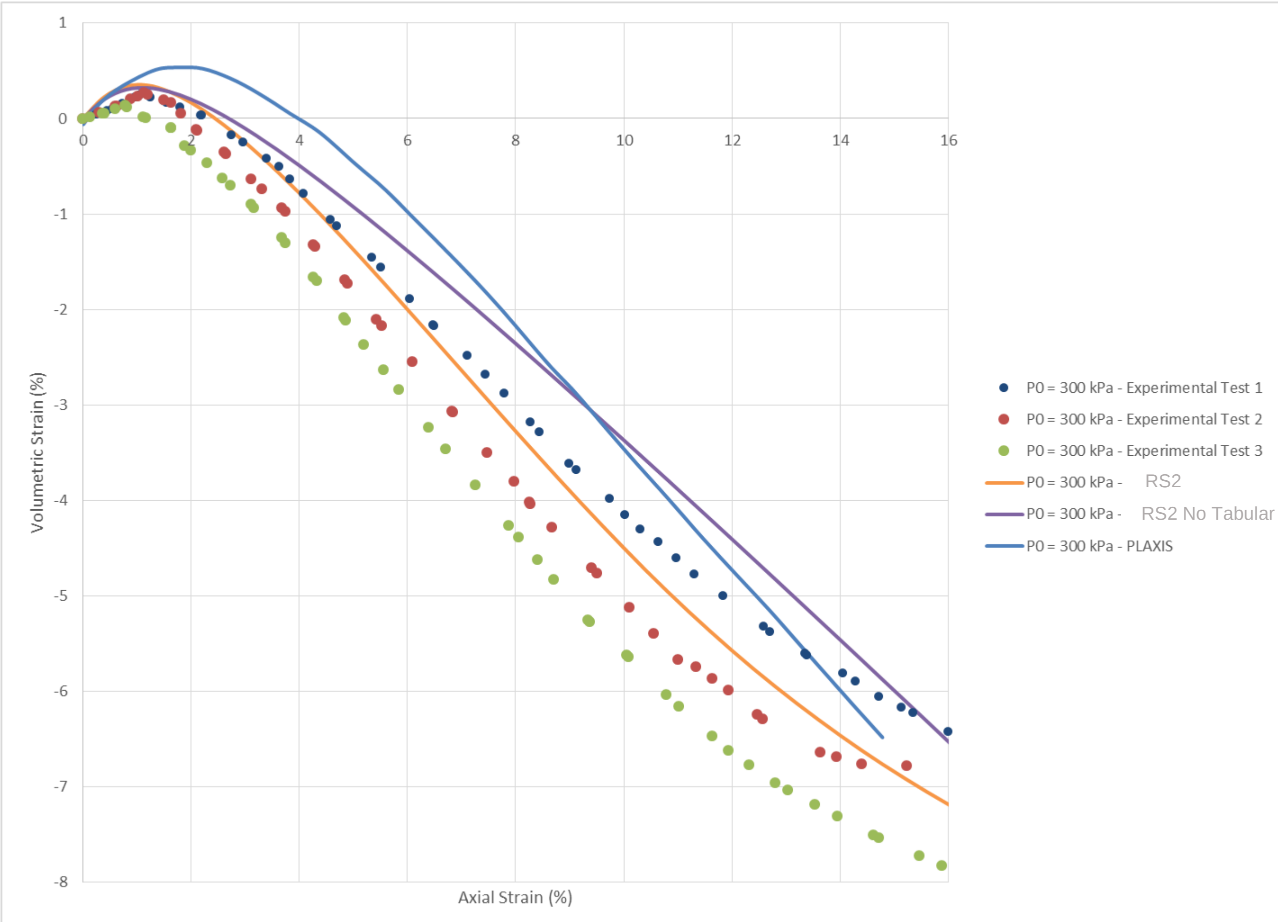

Figure 23: Graph of Volumetric Strain versus Axial Strain for the dense Hostun sand, comparing the RS2 model results, the PLAXIS model results and the experimental data.

1.4.1.5 Loose Hostun Sand

Figure 24 shows the graph of deviatoric stress versus axial strain for the loose Hostun sand. The results from the RS2 model are in close agreement with the experimental data. The RS2 and PLAXIS curves are similar for this test. Similar to the dense Hostun sand tests, the experimental triaxial test was repeated three times, producing three different sets of data.

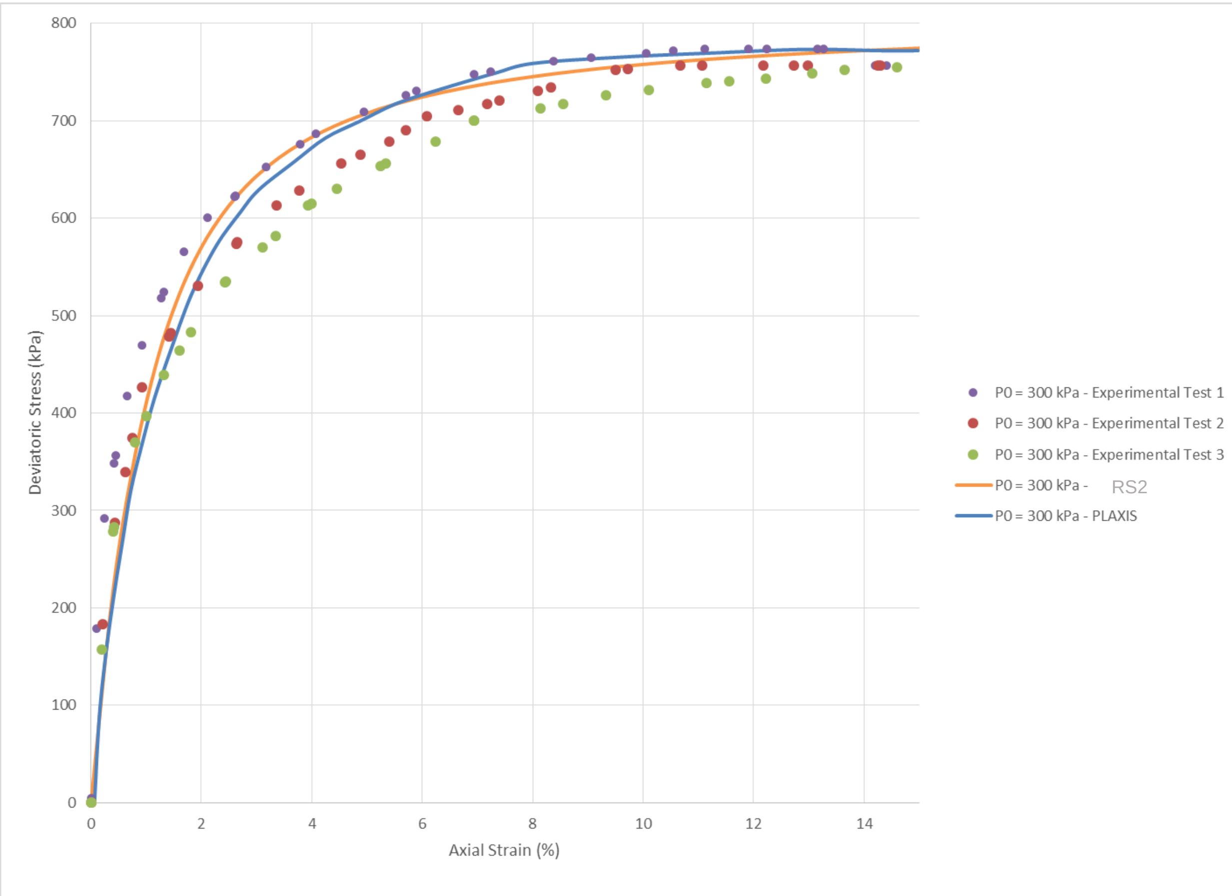

Figure 24: Graph of Deviatoric Stress versus Axial Strain for the loose Hostun sand, comparing the results of the RS2 model, PLAXIS model and the experimental data.

The next figure shows the graph of Volumetric Strain versus Axial Strain, comparing the results of the RS2 model with the experimental data. Similar to the dense Hostun sand tests, the results of the RS2 model are in close agreement with the experimental data. The PLAXIS model results underestimate the volumetric strain at higher axial strains.

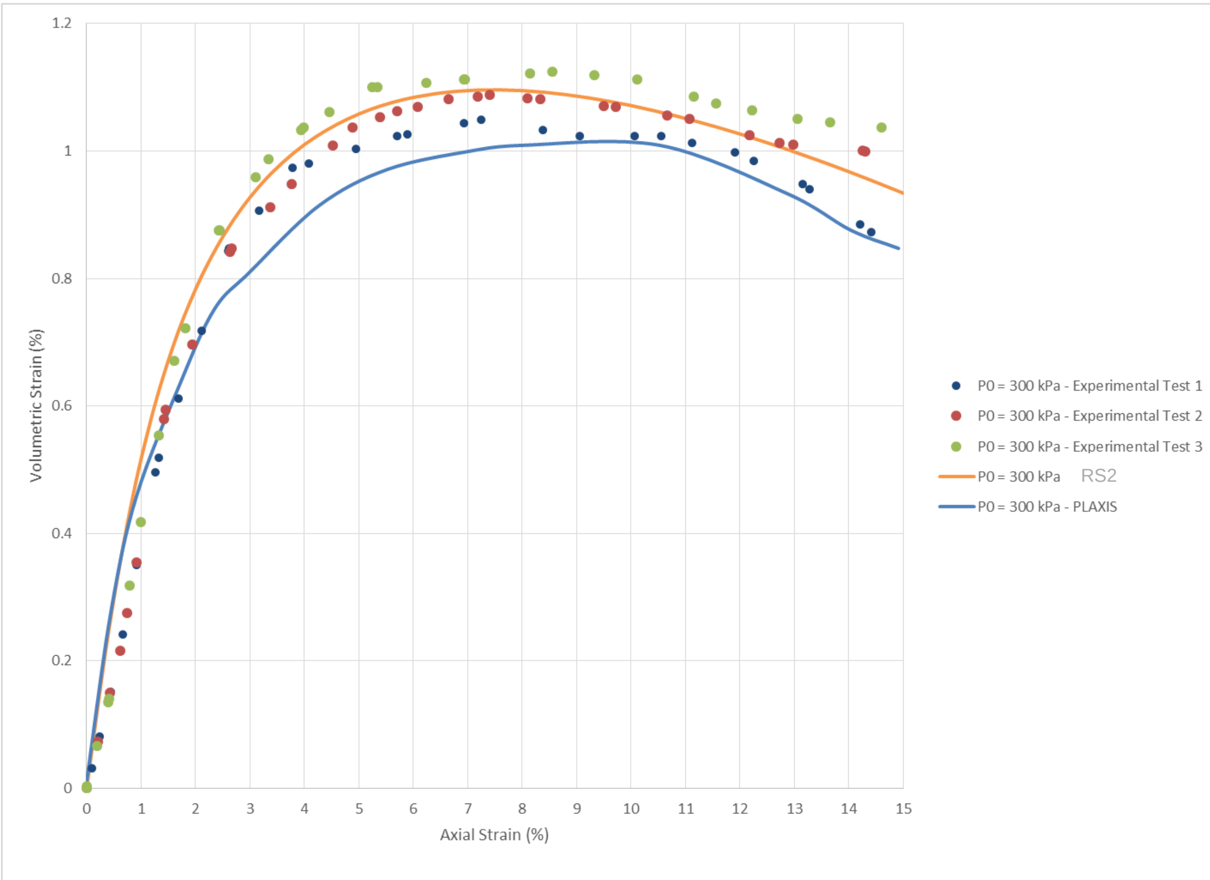

Figure 25: Graph of Volumetric Strain versus Axial Strain for the loose Hostun sand, comparing the RS2 model results, the PLAXIS model results and the experimental data.

1.4.2 Undrained Triaxial Tests

1.4.2.1 Banding Sand

The following figure compares the plots of deviatoric stress versus deviatoric strain between the experimental data and the results of the RS2 model. The results are in fairly good agreement; the differences may be due to the fact that experimental data is being used, or because the model assumed a constant Young's modulus while in reality the Young's modulus varies with stress.

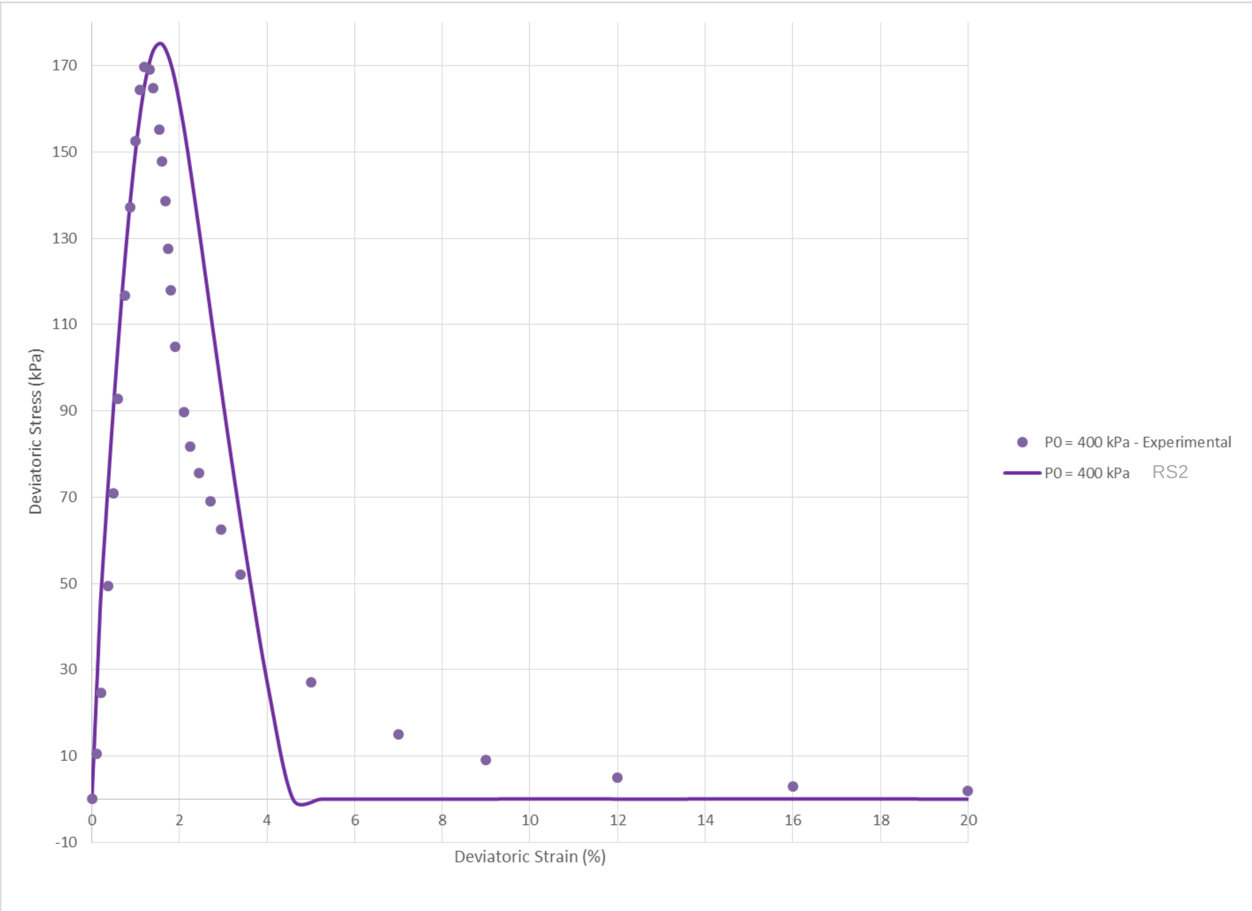

Figure 26: Graph of Deviatoric Stress versus Deviatoric Strain, comparing the experimental data with the RS2 model results for the Banding sand.

The next figure shows the plot of Deviatoric Stress versus Effective Pressure for the two sets of results. Once again the RS2 model is in fairly good agreement with the experimental data, but there are some differences due to the reasons mentioned above.

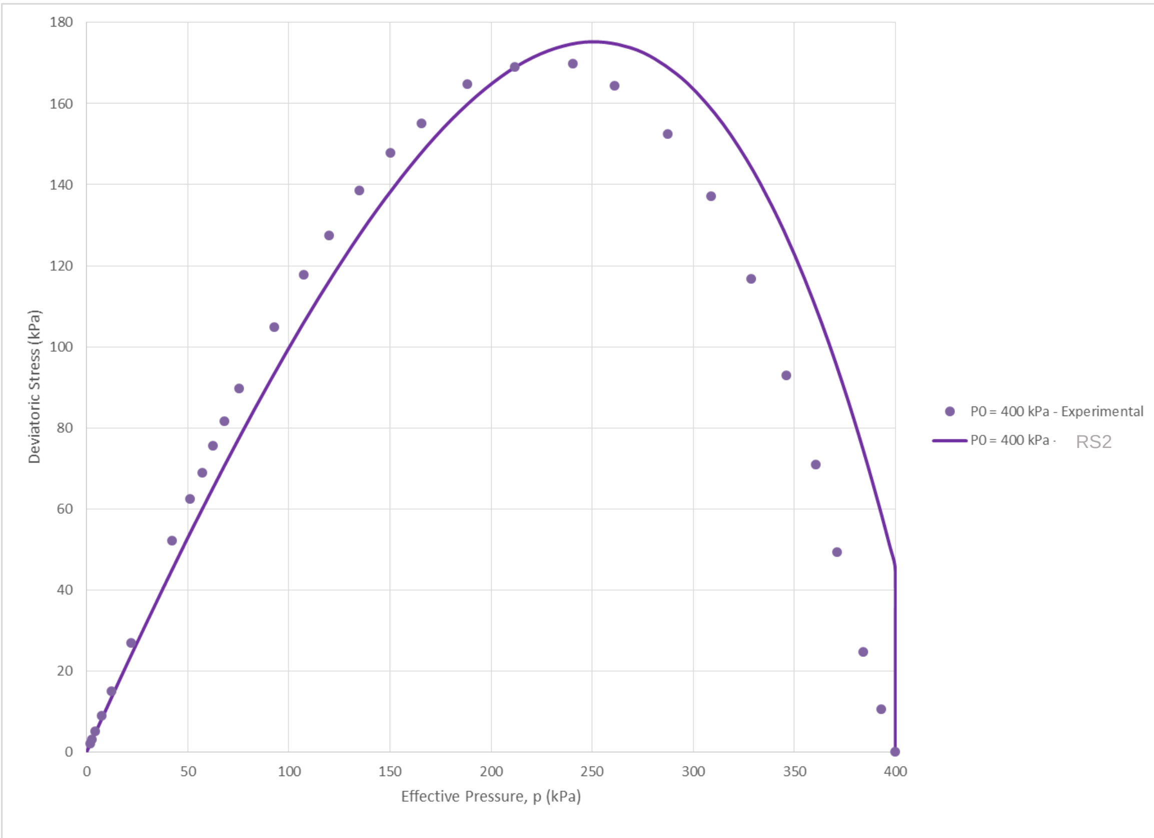

Figure 27: Graph of Deviatoric Stress versus Effective Pressure, comparing the experimental data with the results of the RS2 model for the Banding sand.

The final graph compares the Excess Pore Water Pressure versus Deviatoric Strain results between the experimental data and the RS2 model. The two sets of results are in close agreement with some discrepancies, possibly due to the reasons given above.

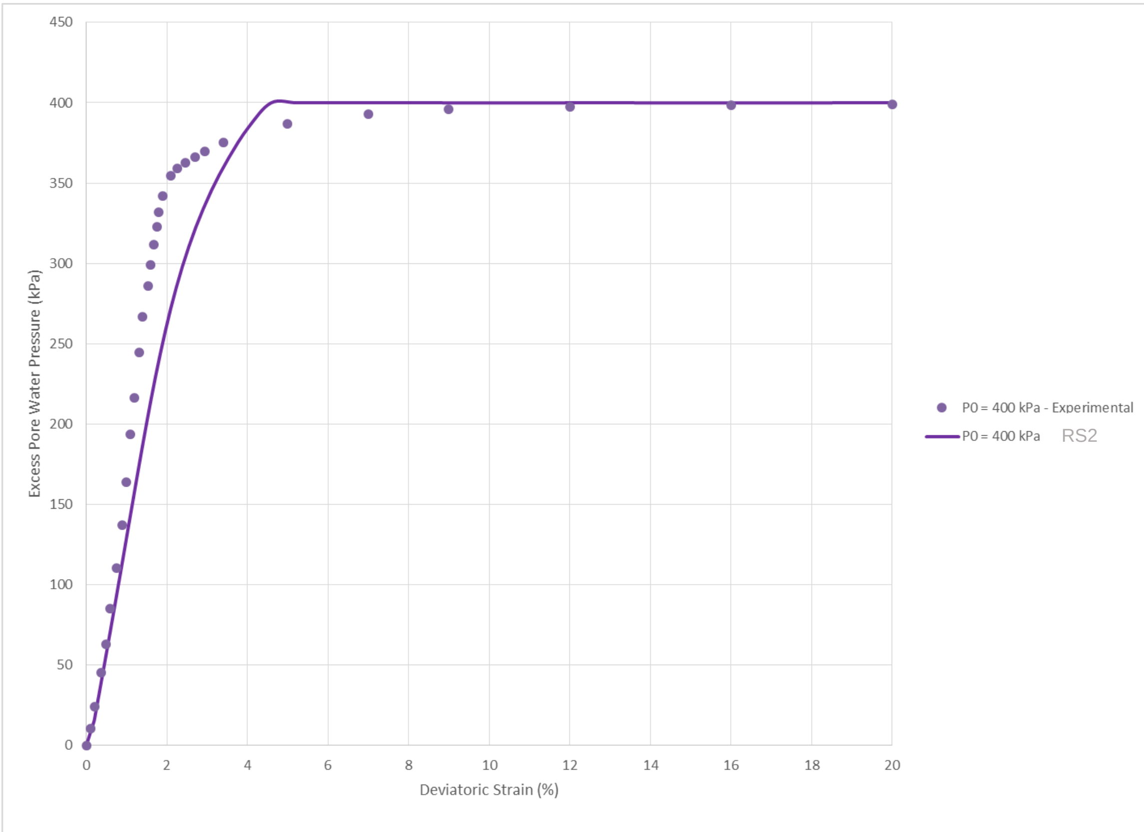

Figure 28: Graph of Excess Pore Water Pressure versus Deviatoric Strain, comparing the results of the RS2 model with the experimental data for the Banding sand.

1.4.2.2 Medium Dense Reid Bedford Sand

The first figure shows the graphs of Deviatoric Stress versus Effective Mean Stress for the experimental data and the RS2 model results at confining stress values of 275 kPa and 550 kPa. The two sets of results are in close agreement. There are some differences, which again are likely due to the fact that a constant value of Young's modulus was used in the model while in reality the value varies with stress, as well as due to the expected variability in experimental results.

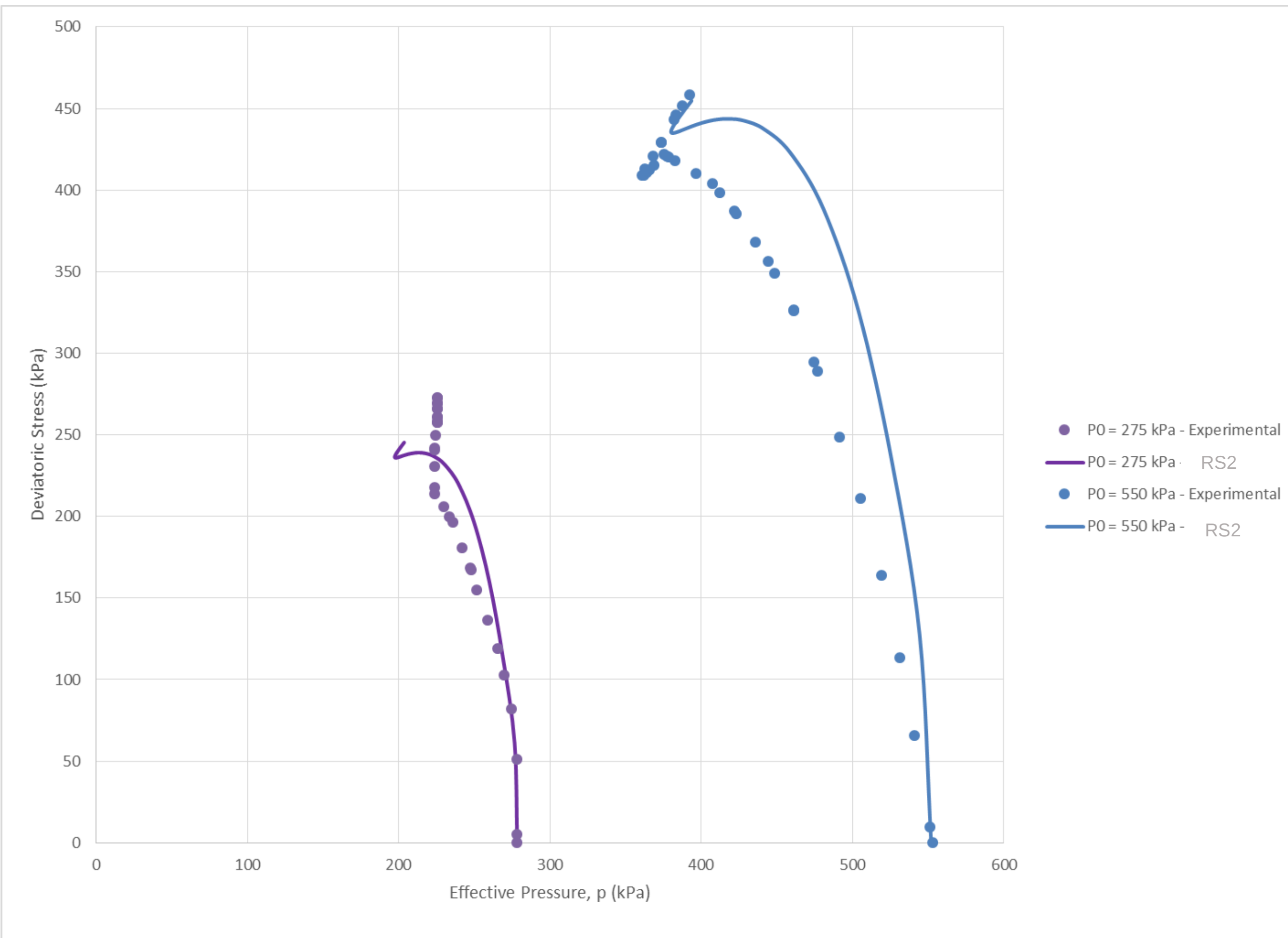

Figure 29: Graph of Deviatoric Stress versus Effective Pressure, comparing the results of the RS2 model with the experimental data for the loose Reid Bedford sand.

The next figure compares the graphs of deviatoric stress versus deviatoric strain for confining stresses of 275 kPa and 500 kPa. The two sets of results are in fairly close agreement, with some minor differences due to the reasons given above.

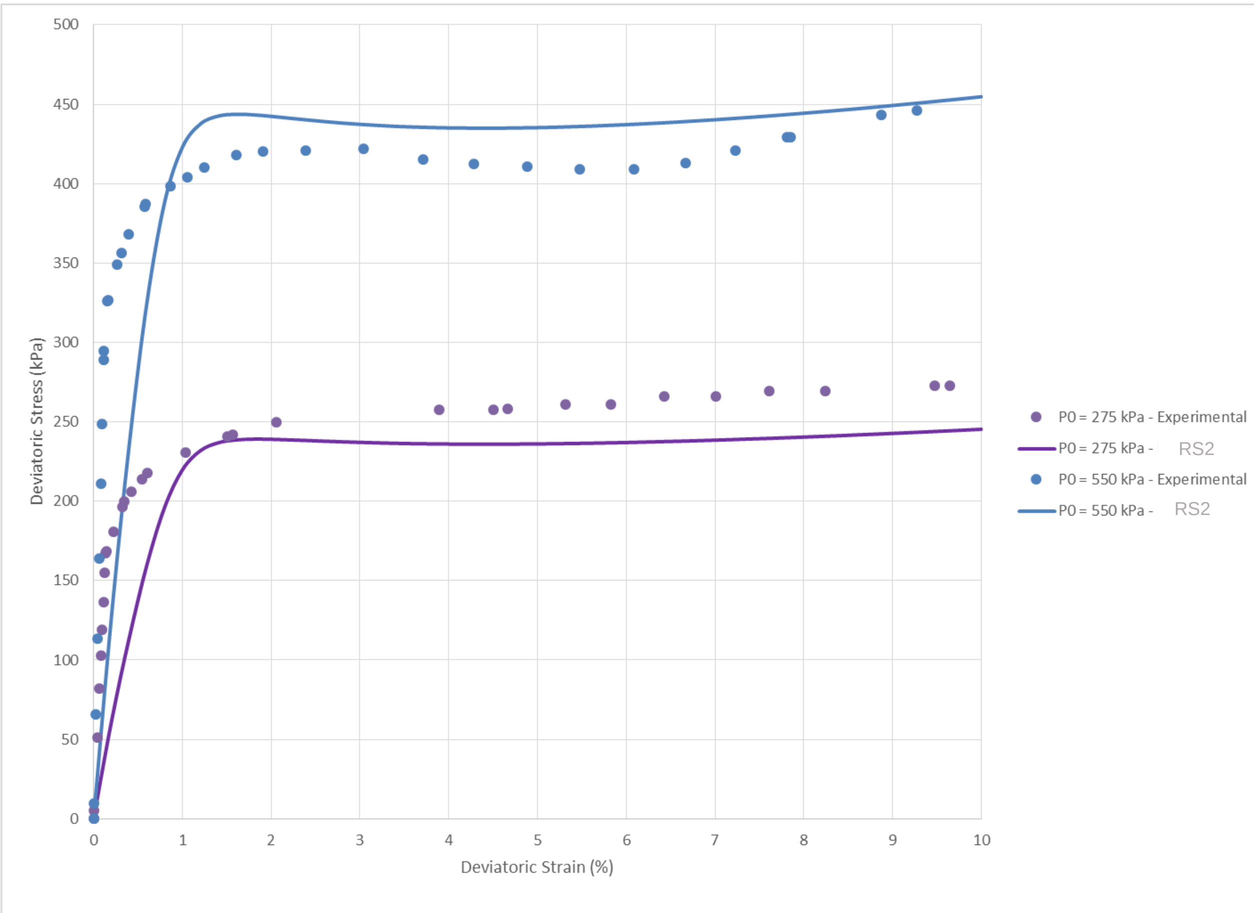

Figure 30: Graph of Deviatoric Stress versus Deviatoric Strain, comparing the results of the RS2 model with the experimental data for the loose Reid Bedford sand.

The final figure compares the graphs of excess pore water pressure versus deviatoric strain for the experimental data and the RS2 model results. Similar to the other graphs, the results are in fairly close agreement.

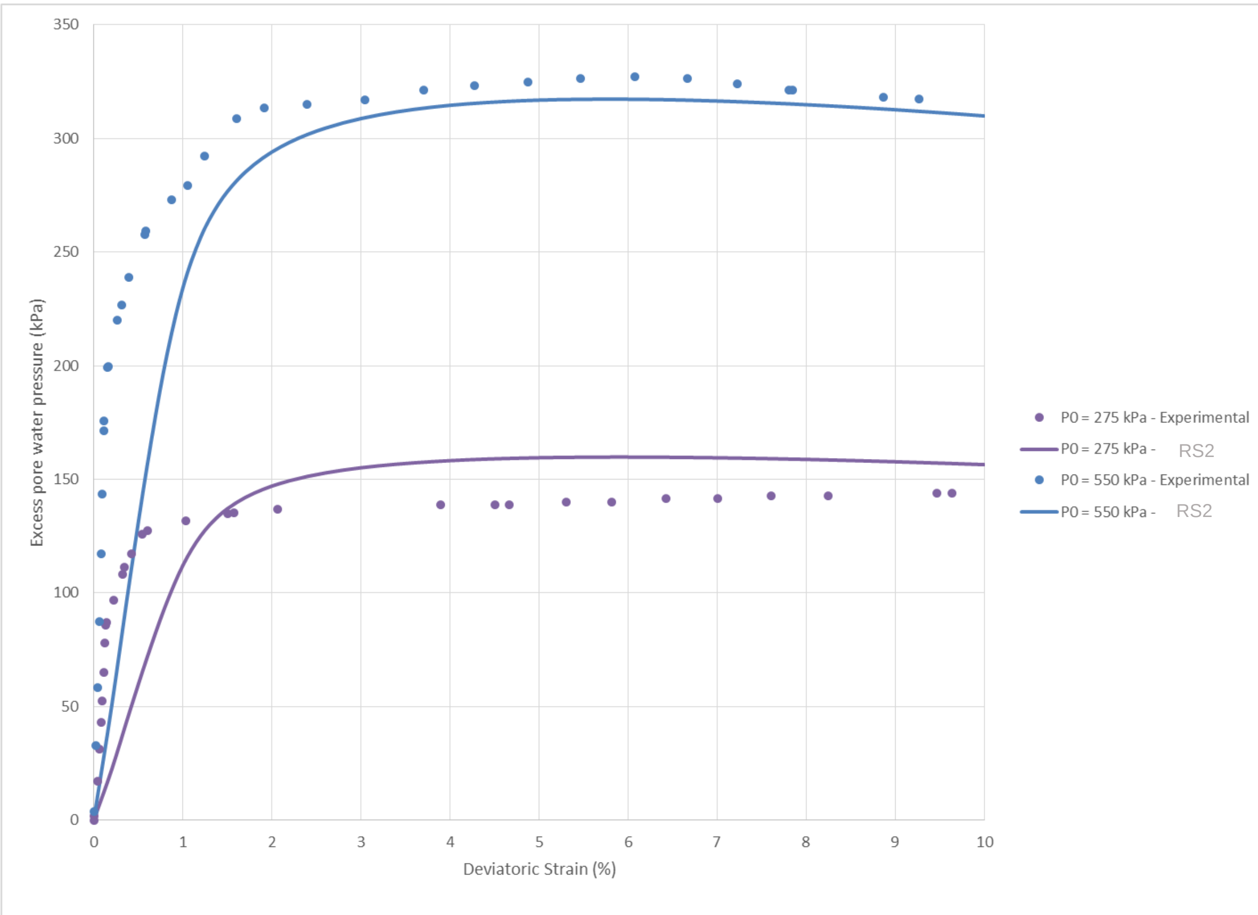

Figure 31: Graph of Excess Pore Water Pressure versus Deviatoric Strain, comparing the experimental data with the results of the RS2 model for the loose Reid Bedford sand.

1.5 References

[1] D. Kolymbas and W. Wu (1990), “Recent Results of Triaxial Tests with Granular Materials”, Powder Technology, 60, 99-119.

[2] K. Alshibli and S. Sture (2000), “Shear Band Formation in Plane Strain Experiments of Sand”, Journal of Geotechnical and Geoenvironmental Engineering, 126, 495-503.

[3] T. Schanz and P.A. Vermeer (1996), “Angles of friction and dilatancy of sand”, Géotechnique, 46, 145-151.

[4] S. Pietruszczak (2010), Fundamentals of Plasticity in Geomechanics, Leiden, The Netherlands: CRC Press.

[5] L. Widulinski, J. Kozicki and J. Tejchman (2009), “Numerical Simulations of Triaxial Test with Sand Using DEM”, Archives of Hydro-Engineering and Environmental Mechanics, 56, 149-171.